Wind and Structures, *Vol. 30, No. 6 (2020) 633-648*
DOI: https://doi.org/10.12989/was.2020.30.6.633

Vortex induced vibration and flutter instability of two parallel cable-stayed bridges

Jirawat Junruang[a] and Virote Boonyapinyo*

Department of Civil Engineering, Thammasat University, Rangsit Campus, Pathumthani, 12120, Thailand

(*Received September 2, 2019, Revised March 10, 2020, Accepted March 19, 2020*)

Abstract. The objective of this work was to investigate the interference effects of two-parallel bridge decks on aerodynamic coefficients, vortex-induced vibration, flutter instability and flutter derivatives. The two bridges have significant difference in cross-sections, dynamic properties, and flutter speeds of each isolate bridge. The aerodynamic static tests and aeroelastic tests were performed in TU-AIT boundary layer wind tunnel in Thammasat University (Thailand) with sectional models in a 1:90 scale. Three configuration cases, including the new bridge stand-alone (case 1), the upstream new bridge and downstream existing bridge (case 2), and the downstream new bridge and the upstream existing bridge (case 3), were selected in this study. The covariance-driven stochastic subspace identification technique (SSI-COV) was applied to identify aerodynamic parameters (i.e., natural frequency, structural damping and state space matrix) of the decks. The results showed that, interference effects of two bridges decks on aerodynamic coefficients result in the slightly reduction of the drag coefficient of case 2 and 3 when compared with case 1. The two parallel configurations of the bridge result in vortex-induced vibrations (VIV) and significantly lower the flutter speed compared with the new bridge alone. The huge torsional motion from upstream new bridge (case 2) generated turbulent wakes flow and resulted in vertical aerodynamic damping $H1^*$ of existing bridge becomes zero at wind speed of 72.01 m/s. In this case, the downstream existing bridge was subjected to galloping oscillation induced by the turbulent wake of upstream new bridge. The new bridge also results in significant reduction of the flutter speed of existing bridge from the 128.29 m/s flutter speed of the isolated existing bridge to the 75.35 m/s flutter speed of downstream existing bridge.

Keywords: wind tunnel; parallel cable-stayed bridges; vortex induced vibration; flutter derivatives; covariance-driven stochastic subspace identification

1. Introduction

Recently, the trend of construction project for long span bridges such as suspension bridges and cable-stayed bridges is parallel bridge configurations due to increasing transportation demand. Examples of a parallel bridge deck around the world include the New Tacoma bridges in the USA (Irwin *et al*. 2005), the J.P. Duarte bridge in St. Domingo (Larsen *et al*. 2000), the Haihe and the Hongdao bridges in China (MENG *et al*. 2011, LIU *et al*. 2009) and the Jindo bridge in Korea (Seo *et al*. 2013, Kim *et al*. 2013, Park *et al*. 2017, Park and Kim 2017). Typically, long-span bridges are very flexible and low structural damping. The wind induced responses for parallel bridge configurations become more complicated than single bridge configurations. The main issues are focusing on the serviceability, safety and sustainability of parallel bridges against wind excitation. In the wind resistance analysis of parallel bridges, interference effect on aerodynamic coefficient, vortex-induced vibration (VIV) and flutter instability are the key parameters need to be study.

Previous studies reported the interference effects on aerodynamic coefficients and vortex-induced vibration (VIV) of parallel cable-stayed bridges. The first parameter on parallel bridges need to be investigated is the aerodynamic coefficients. The main effect is a reduction in a drag force of the deck in parallel bridge configurations that was much smaller than that in the single bridge configurations (Argentini *et al*. 2015, Larsen *et al*. 2000, Liu *et al*. 2009). The aerodynamic interference effects on lift and torque coefficients of twin decks can be neglected (Liu *et al*., 2009).

The next issues on parallel bridges need to be investigated is vortex-induced vibration (VIV). Shapes of the bridges, dynamic characteristics and a gap width between parallel decks are the main factors that affect VIV in a parallel cable-stayed bridge (Kimura *et al*. 2008, Seo *et al*. 2013, Kim *et al*. 2013, Argentini *et al*. 2015, Park *et al*. 2017, Park and Kim 2017). The effects of parallel decks with difference cross section can be significant even with a separation distance as large as 8 times the deck width (Kimura *et al*., 2008). the gap distances of five to seven times the depth of the upstream deck critically affected the interactive VIV in twin parallel cable-stayed bridges (Park *et al*. 2017). Heaving motion in actual upstream parallel twin Jindo bridge exceeds the allowable limit for serviceability performance and reproduced VIV in wind tunnel (Seo *et al*. 2013). The particle image velocimetry (PIV) measurements was measured to visualized the flow

*Corresponding author, Ph.D. Associate Professor
E-mail: bvirote@engr.tu.ac.th
[a]Ph.D. Student
E-mail: jbjirawat@gmail.com

http://www.techno-press.com/journals/was&subpage=7
ISSN: 1226-6116 (Print), 1598-6225 (Online)

(a) The original stand-alone configuration

(b) Image of the new bridge (behind) with the existing bridge (front)

Fig. 1 The Rama IX bridge in Thailand

pattern between parallel decks (Seo *et al*. 2013, Park *et al*. 2017). The difference dynamic characteristics in term of frequency ratio (the ratio of the natural frequency of the upstream deck to that of the downstream deck) affected the interactive VIV in twin parallel cable-stayed bridges (Park and Kim 2017). There was the interactive phenomenon in VIV of parallel decks (Argentini *et al*. 2015, Dallaire *et al*. 2016). The computational fluid dynamic method (Dragomirescu *et al*. 2016, Laima *et al*. 2019) was applied to follow the flow mechanism of aerodynamic interference phenomena which observed in wind tunnel test (MENG *et al*. 2011). It can be seen that the previous research focused on the behavior of the aeroelastic interference on VIV, which is just one of many key factors for design wind resistance of parallel cable-stayed bridges.

Flutter instability is the main reason of failure for the long-span bridges. Several researchers use wind tunnel tests for studying flutter performance of long-span bridges (Hu *et al*. 2019, Wang *et al*. 2019). The determination of flutter derivative by wind tunnel tests can be divided into two type includes forced and free vibration. The buffeting test method is simple, cost effective and closely related to the real bridge behavior. However, this method needs an advance system identification. The advance covariant-driven stochastic system identification method was used to determine the flutter derivative by many researcher (Gu *et al*. 2001, 2004, Boonyapinyo and Janesupasaeree 2010, Andersen *et al*. 2018). This method exhibits a good result with numerical simulations of the bridge deck, experimental for thin plate model and Industrial-Ring-Road (IRR) bridge model (Boonyapinyo and Janesupasaeree, 2010). Nowadays, the information available on the flutter instability and flutter derivative of parallel cable stayed bridges are few and need more researchers.

The main objective of this study was to investigate the interference effects between Rama IX parallel cable-stayed bridges with difference cross section on aerodynamic coefficient, VIV, flutter instability and flutter derivative by wind tunnel tests. In previous studies, one of the parallel section models test was set at heaving motion or fixed to simplified the experimental setup (Kimura *et al*., 2008, Seo *et al*. 2013), the interested section model was s*et al*low to move heaving and torsion (2 degrees of freedom). In this research, both two section models in a 1:90 scale were elastically supported to allow heaving and torsion (2 degrees of freedom) motion for two parallel cable-stayed bridge models. Three configuration cases, including the new bridge stand-alone (case 1), the upstream new bridge and downstream existing bridge (case 2), and the downstream new bridge and the upstream existing bridge (case 3) were selected in this study. The SSI-COV method was used to estimate the flutter derivatives from random responses (buffeting) under the action of smooth wind. All tests were conducted in TU-AIT boundary layer wind tunnel in Thammasat University, Thailand.

2. Description of the two parallel cacle-stayed bridge

The existing Rama IX bridge (see Fig. 1(a)) carries six lanes of expressway traffic across the Chao Phraya River in Bangkok, Thailand. It connected the Yan Nawa District to Rat Burana District as a part of the Dao Khanong - Port Section of Chalerm Maha Nakhon Expressway. The bridge opened to traffic in 1987, with a 450 m long cable-stayed section over the river and two 166-meter side spans. The deck is a steel box girder with orthotropic deck and steel pylons are supported on concrete piers and pile foundations.

The Expressway and Rapid Transit Authority of Thailand (ETA) plan to build a new bridge which parallel to the old bridge (see Fig. 1(b)). The new Rama ix bridge carries eight lanes of expressway and constructed to solve traffic congestion from Thonburi side to the city of Bangkok. The new bridge is a cable-stayed bridge, with two longitudinal steel box girders connected by transverse steel cross beam spread evenly along the bridge. The dimensions of the two decks are shown in Fig.2 and the layout of the existing Bridge and the new Rama IX Bridge are shown in Fig. 3.

The targets of the wind tunnel experimental were to assess the interference of the existing bridge on the new bridge, and via versus in terms of effects on aerodynamic coefficients, vortex-induced vibrations, flutter instability and flutter derivative.

3. Wind tunnel tests

In order to study the interferences effect of two parallel decks on aerodynamic static and aeroelastic, the test of two-edge girder type blunt section models (see Fig. 4) were performed in TU-AIT boundary layer wind tunnel in Thammasat University, Thailand. The working section of wind tunnel has a width of 2.5 m, a height of 2.5 m., a

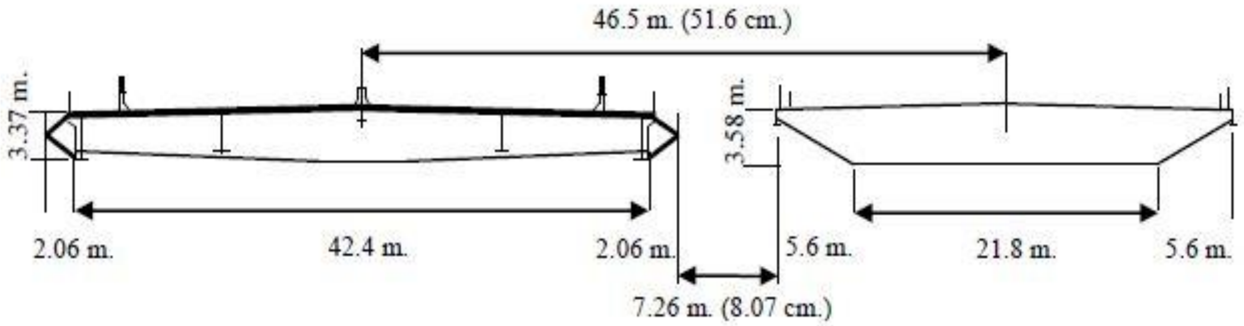

(a) New bridge (b) Existing bridge

Fig. 2 Cross section of prototype and position of two parallel bridge deck sections (Dimension for the scaled model are shown in parentheses

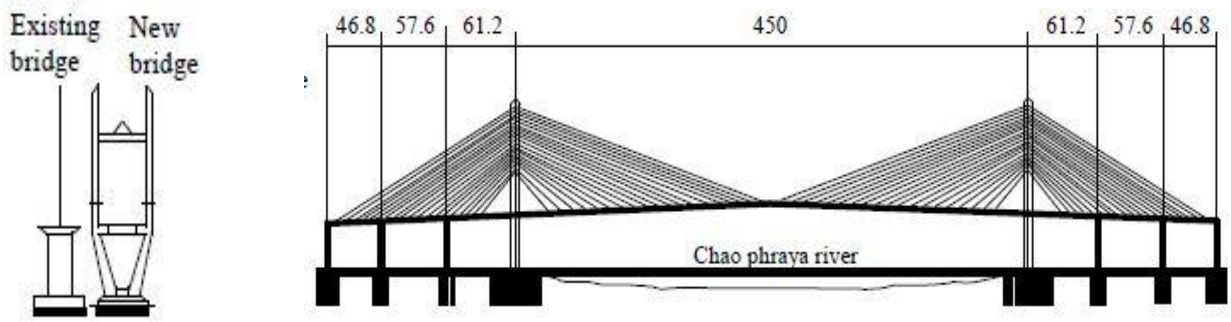

(b) Elevation view of towers (a) Elevation view

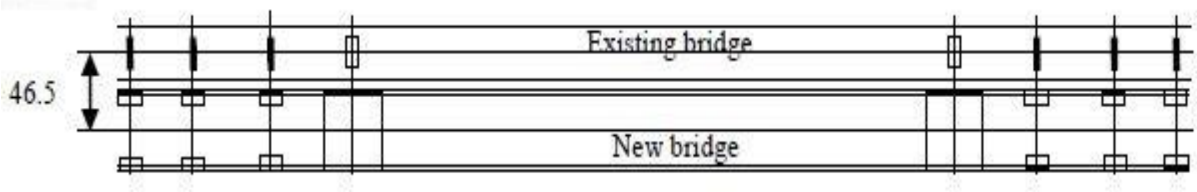

(c) Plan view

Fig. 3 Layout of the existing and the new Rama IX bridge (unit: m.)

length of 25.5 m. and wind speed is in the range of 0.5 to 20 m/s. A 1:90 geometrically scaled section models of the two bridges were constructed by aluminum and acrylic. The length of the section model was selected as 2.26 m to be compatible with the wind tunnel used. All details were scaled down geometrically, with exception of some details such as railings that use equivalent area. Dynamic properties of the existing Rama IX cable-stayed bridges were obtained from the Rama IX Bridge Tenth-Year Inspection (2001). In addition, the main span of new bridge has the same length of existing bridge (450 m.) but the deck width is 42.4 m (see Figs. 2 and 3). The gap distance between two bridges is 7.26 m. Dynamic properties of the new Rama IX cable-stayed bridges were obtained from the Epsilon Co. Ltd. and Weicon Co. Ltd. (2016). Table 1 list the main parameters of the actual bridge and the section model of the new and existing bridge, respectively. The length scale λ_L = 1:90, frequency scale λ_f = 7.32, velocity scale λ_V = 12.28 and modal damping ξ_h = 0.23%, ξ_α = 0.14% for new bridge. The length scale λ_L = 1:90, frequency scale λ_f = 7.25, velocity scale λ_V = 12.40 and modal damping ξ_h = 0.45%, ξ_α = 0.31% for existing bridge.

3.1 Aerodynamic static measurements by wind tunnel tests

The aerodynamic static measurements, the section model was fixed to the force gauges sensors (JR3 sensor, Model No. 5492 and 2873) at both ends of section model (See in Fig. 5(b)) and connected to External Electronic Box of JR3 sensor by a special cable provided. Overload Alarm & Power supply were also connected to External Electronic Box. Analog signals from External Electronic Box were then passed through analogue amplifiers and filter, digitized by A/D converter and stored in PC by special software (LabView). The mean values of the voltage outputs of the lift, moment and drag channels from sensors were recorded. These voltage outputs at each wind speed and angle of attack were converted to mean forces values by multiplying the sensor's calibration matrix, which were found separately,

Table 1 Dynamic parameters for the sectional model

Parameters	Similarity scale	New Rama IX bridge		Existing Rama IX bridge	
		Prototype	Model	Prototype	Model
Length (m.)	λ_L	-	2.26	-	2.26
Width (m.)	λ_L	42.4	0.471	33	0.367
Height (m.)	λ_L	3.87	0.043	4	0.045
Mass (kg/m.)	λ_L^2	58486	7.05	25467	3.10
Mass moment of inertia (kg m^2/m)	λ_L^4	7571830	0.1123	2010000	0.0309
First vertical frequency (Hz.)	λ_f	0.291	2.132	0.32	2.322
First torsional frequency (Hz.)	λ_f	0.416	3.034	0.67	4.903
Torsional to vertical frequency ratio	1	1.43	1.42	2.09	2.11
Vertical damping ratio (%)	1	0.40	0.25	0.40	0.45
Torsional damping ratio (%)	1	0.25	0.14	0.25	0.31

(a) Bottom view of the two-sectional model

(b) Top view of the two-sectional model

Fig. 4 Section model in wind tunnel

(a) Aeroelastic rig support

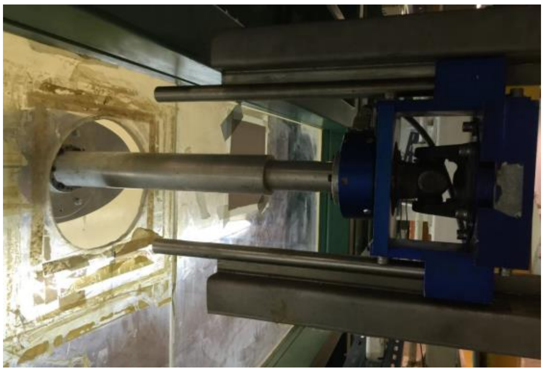

(b) Aerodynamic static rig support

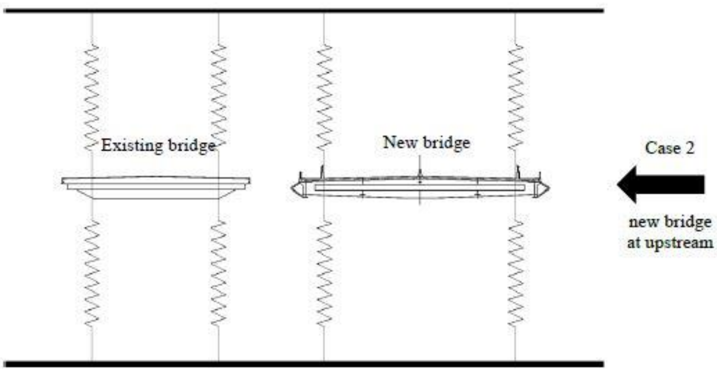

(c) Setup for aeroelastic test for two parallel bridges in wind tunnel

Fig. 5 Setup of wind tunnel tests for two parallel bridges

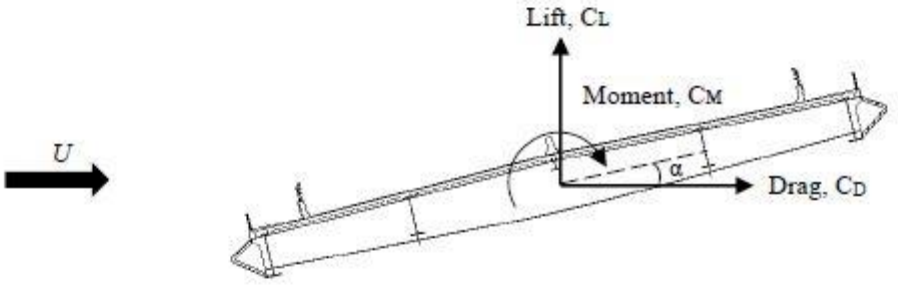

Fig. 6 Sign conventions for aerodynamic coefficients

with mean value of output voltages. Summing of mean forces at both ends yield the total forces act upon the model.

3.2 Aeroelastic measurements by wind tunnel tests

In the aeroelastic measurements, the section model was installed in the dynamic rig about the center of rotation of the section suspended from a set of four supports as shown in Figs. 5(a) and 5(c) with upper and lower springs at each support. Thus, it can oscillate vertically and in torsion (about a transverse axis). Piano wires were used to arrest the motion of the model in the along-wind direction. The vertical length of the spring can be adjusted to set proper vertical frequency. The torsional frequency is set by adjusting spacing between the springs at each end of the model. Two acceleration transducers were used in recording acceleration time histories at the mid-section of the model. The acceleration sensor consisted of the acceleration transducer model AS-2GB, the PCD 300A sensor interface and control software. The transducer has almost constant frequency response (within ± 5%) up to 1000 Hz.

4. Covariance-driven stochastic subspace identification for flutter derivatives

Base on the dynamic behavior of a bridge deck with two degrees-of-freedom (DOF in short), i.e. h (bending) and α (torsion), in turbulent flow can be described by the following differential equations of equilibrium. The self-excited lift and moment are given as follows by Simiu and Scanlan (1996):

$$L_{se}(t) = \frac{1}{2}\rho U^2 B\left[K_h H_1^*(K_h)\frac{\dot{h}}{U}+K_\alpha H_2^*(K_\alpha)\frac{B\dot{\alpha}}{U}+K_\alpha^2 H_3^*(K_\alpha)\alpha+K_h^2 H_4^*(K_h)\frac{h}{B}\right]$$
$$M_{se}(t)= \frac{1}{2}\rho U^2 B^2\left[K_h A_1^*(K_h)\frac{\dot{h}}{U}+K_\alpha A_2^*(K_\alpha)\frac{B\dot{\alpha}}{U}+K_\alpha^2 A_3^*(K_\alpha)\alpha+K_h^2 A_4^*(K_h)\frac{h}{B}\right] \quad (1)$$

where ρ is air mass density; B is the width of the bridge deck; U is the mean wind speed at the bridge deck level; $k_i=\omega_i B/U$ is the reduced frequency ($i=h,\alpha$); H_i* and A_i* ($i=1,2,3,4$) are the so-called flutter derivatives, which can be regarded as the implicit functions of the deck's modal parameters. By moving L_{se} and M_{se} to the left side, and merging the congeners into column vectors or matrices, dynamic equation of equilibrium can be rewritten as follows:

$$[M]\{\ddot{y}(t)\}+\left[C^e\right]\{\dot{y}(t)\}+\left[K^e\right]\{y(t)\}=\{f(t)\} \quad (2)$$

The fluctuations of wind speed u(t) and w(t) in are random functions of time, so the identification of flutter derivatives of bridge decks can be simplified as a typical inverse problem in the theory of random vibration, and thus can be solved by stochastic system identification techniques.

$$\text{Let}\quad [A_c]=\begin{bmatrix} \mathrm{O} & \mathrm{I} \\ -M^{-1}K^e & -M^{-1}C^e \end{bmatrix}$$
$$[C_c]=[\mathrm{I}\quad \mathrm{O}] \quad (3)$$
$$\text{And}\quad \{x\}=\begin{Bmatrix} y \\ \dot{y} \end{Bmatrix}$$

Then, Eq. (2) is transformed into the following stochastic state equation in discrete form as

$$\{x_{k+1}\}=[A]\{x_k\}+\{w_k\}\,and\,\{y_k\}=[C]\{x_k\}+\{v_k\} \quad (4)$$

The SSI-COV algorithm, the raw time histories are converted to the covariances of the Toeplitz matrix. The implementation of SSI-COV consists of estimating the covariances, computing the singular value decomposition (SVD) of the Toeplitz matrix, truncate the SVD to the model order n, estimating the observability and the controllability matrices by splitting the SVD into two parts, and finally estimating the system matrix (A, C). The modal parameters are found from A and C.

Once the modal parameters are identified, the gross damping matrix C^e and the gross stiffness matrix K^e can be readily determined by the pseudo-inverse method. Let: $\overline{C^e}=M^{-1}C^e$, $\overline{K^e}=M^{-1}K^e$, $\overline{C}=M^{-1}C^0$ and $\overline{K}=M^{-1}K^0$ where C^0 and K^0 are the 'inherent' damping and stiffness matrices, respectively. Thus, the flutter derivatives can be extracted from the following equations.

$$H_1^*(k_h) = -\frac{2m}{\rho B^2 \varpi_h}(\overline{C_{11}^e} - \overline{C_{11}^0}) \qquad A_1^*(k_h) = -\frac{2I}{\rho B^3 \varpi_h}(\overline{C_{21}^e} - \overline{C_{21}^0})$$

$$H_2^*(k_\alpha) = -\frac{2m}{\rho B^3 \varpi_\alpha}(\overline{C_{12}^e} - \overline{C_{12}^0}) \qquad A_2^*(k_\alpha) = -\frac{2I}{\rho B^4 \varpi_h}(\overline{C_{22}^e} - \overline{C_{22}^0})$$

$$H_3^*(k_\alpha) = -\frac{2m}{\rho B^3 \varpi_\alpha^2}(\overline{K_{12}^e} - \overline{K_{12}^0}) \qquad A_3^*(k_\alpha) = -\frac{2I}{\rho B^4 \varpi_h^2}(\overline{K_{22}^e} - \overline{K_{22}^0}) \tag{5}$$

$$H_4^*(k_h) = -\frac{2m}{\rho B^3 \varpi_h^2}(\overline{K_{11}^e} - \overline{K_{11}^0}) \qquad A_4^*(k_\alpha) = -\frac{2I}{\rho B^4 \varpi_h^2}(\overline{K_{21}^e} - \overline{K_{21}^0})$$

For more information about SSI-COV algorithm and identification method of flutter derivative of bridge deck have been reported by Boonyapinyo and Janesupasaeree (2010), among other.

5. Interference effects of two-parallel bridge decks on aerodynamic coefficients of new bridge

In order to studies interference effects on aerodynamic coefficients of new bridge, wind attack angles were varying in steps of 3° from -12° to +12°. In each angle of wind attack, model was subjected to three different wind velocities: U = 3.61, 5.71 and 8.24 m/s. Summing of mean forces at both ends yield the total mean forces act upon the model. The aerodynamic coefficients were then found using Eq. (6) as:

$$C_L = \frac{L}{0.5\rho U^2 Bl} \qquad C_D = \frac{D}{0.5\rho U^2 Bl} \qquad C_M = \frac{M}{0.5\rho U^2 B^2 l} \tag{6}$$

where B and l are the deck width and length of the section model, respectively. L, D, M are total lift forces, drag forces and pitching moment, respectively. The sign convention used in the presentation of the test results is shown in Fig. 6. The aerodynamic coefficients of new bridge in three configuration cases, namely the new bridge stand-alone (case 1), the upstream new bridge and downstream existing bridge (case 2), and the downstream new bridge and the upstream existing bridge (case 3) are given in Fig. 7.

The results showed that a drag coefficient of new bridge in parallel configuration were drop for all attack angles when compare with the isolate New bridge. Drag coefficient of new bridge in case 2 was lowest at attack angle 0° (drop about -10%) and in case 3 was lowest at attack angle -3° (drop about -29%). A drag coefficient of New bridge was drop significantly in case 3 due to the new bridge was sheltered by existing bridge.

Lift coefficient of new bridge in case 2 has the same trend with case 1. The absolute value of the lift coefficient of new bridge in case 2 was lower than case 1 for attack angles -12° to -3° and 3° to 12° but at 0° case 2 was higher than case 1. Case 3 report the same result as case 2 but at 0° the lift coefficient changes from -0.1016 (down forced) to 0.162 (lift forced).

The absolute value of the torsion coefficients of new bridge in case 2 and 3 were quite similar to case 1 while that at -12° to -3° angle of attack was lower than that of case 1. Since the new bridge located at upstream (case 2) at attack angle 3° torsion coefficients changes from 0.0166 (clockwise) to -0.0032 (counter clockwise) was an interest

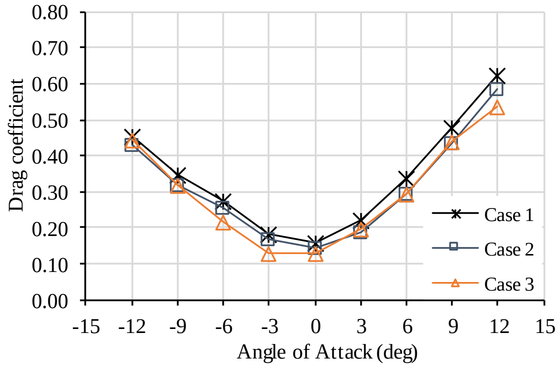

(a) Drag coefficient

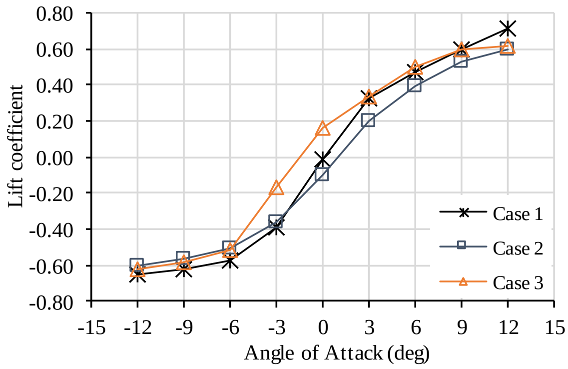

(b) Lift coefficient

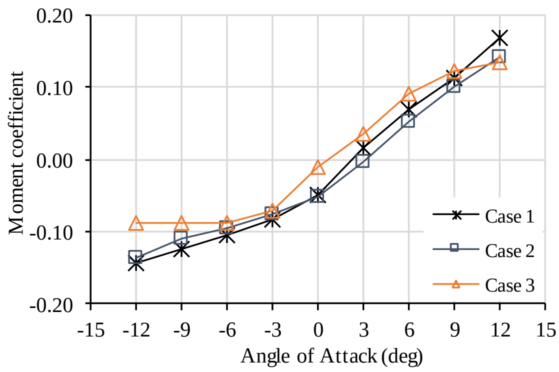

(c) Moment coefficient

Fig. 7 Comparison of C_D, C_L, and C_M of new bridge for three configuration cases

phenomenon.

The aerodynamic coefficients are applied for investigation of the nonlinear aerodynamic instability analysis of long-span bridges (Boonyapinyo *et al.* 1994, 2006)

6. Interferences effects of two-parallel bridge decks on vortex-induced vibration and flutter response

According to the wind-resistant design manual for highway bridges in Japan (Sato, 2003), the allowable amplitudes of new bridge for vertical bending were ((0.04/0.291)*100) = 13.75 cm. in term of maximum

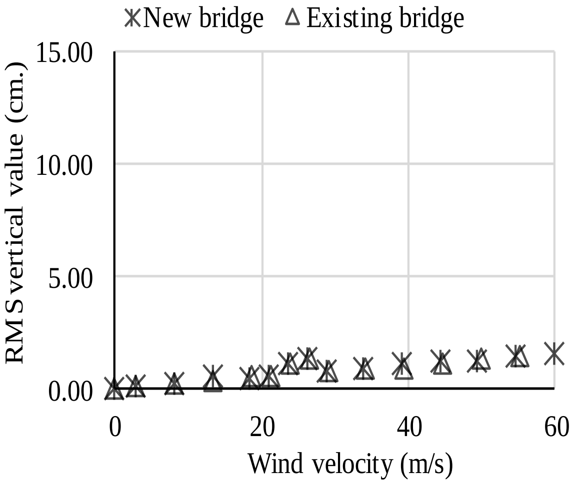

(a) Heave response

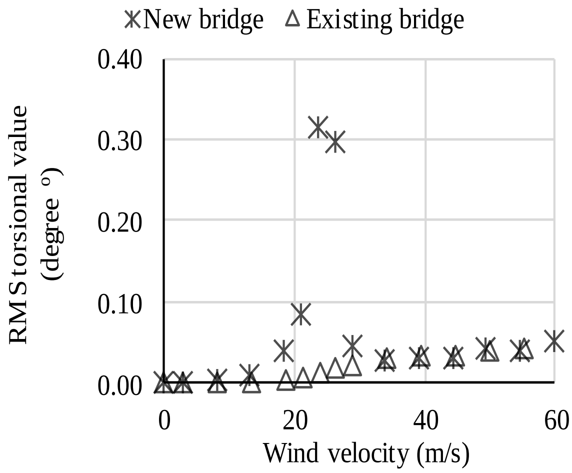

(b) Pitch response

Fig. 8 RMS-velocity curve of new and existing bridges for case 2

vertical displacement, which is equivalent to 9.8 cm. in term of RMS vertical displacement and (2.28/(15.22*0.416)) = 0.36° in term of maximum torsional degree, which is equivalent to 0.25° in term of RMS torsional degree.

For existing bridge, the allowable amplitudes of vertical bending were ((0.04/0.32)*100) = 12.5 cm. in term of maximum vertical displacement, which is equivalent to 8.9 cm. in term of RMS vertical displacement and (2.28/(13.54*0.67)) = 0.25° in term of maximum torsional degree, which is equivalent to 0.17° in term of RMS torsional degree.

It should be note that this research was emphasized on the sectional model test of two parallel bridges. The maximal VIV responses of the full bridge are different from VIV responses directly obtained via sectional model. A modal shape effect (Zhu 2005, Zhang and Chen 2011) and spanwise correlation of the fluctuating wind (Ehsan, F. and Scanlan 1990) which can be obtained based on proper model of vortex-induced force. These effects should be considered in further work when transforming the VIV responses of the sectional model to those of the full bridge.

From the sectional bridge model test in wind tunnel, the new bridge alone (case 1) with fairing and damping ratio (ξ_h = 0.23% for heave and ξ_a = 0.14% for pitching) and the existing bridge alone with damping ratio (ξ_h = 0.45% for heave and ξ_a = 0.31% for pitching) show no problem in vortex-induced vibration. These results agree well with the similar, previous research by Boonyapinyo *et al*. (2009) who investigated the effects of fairing modification on VIV and flutter instability of the Industrial Ring Road Bridge (the Bhumibol Bridge) in Thailand by section model test.

Those results shown that the modified section with fairing can suppress the vortex shedding significantly and slightly increase in flutter speed, compared with original section without fairing. In addition, those results shown that the modified section with fairing and soffit plates can significantly increase in flutter speed, compared with original section without fairing.

However, the interference effects occur when the two decks were located in parallel configurations with ratio between the gap distance of two decks and the width (x = 7.26/42.4 = 0.17, normalize with the width of new bridge). The Interferences effects of two-parallel bridge decks on vortex-induced vibration and flutter response can be summarized as follows.

6.1 Vortex-induced vibration for the upstream new bridge and downstream existing bridge (Case 2)

Response of the new bridge and existing bridge are represented in term of RMS and velocity. Fig 8 show the RMS-velocity of new bridge and existing bridge in case 2. The Strouhal number (St) of new bridge in case 2 (new bridge located at upstream) was measured to be 3.021*0.043/1.924 = 0.067. The VIV occurs at mean wind speed of 23.63 m/s, this vortex-shedding speed is relatively high. The vortex-shedding excitation was also shown in torsional motion of new bridge (See Fig. 9(b)). The maximum RMS vertical value of new bridge was 1.1 cm., this value is significantly lower than that of the 9.8 cm. allowable limit of vibration recommended in the wind-resistant design manual for highway bridges in Japan (Sato 2003) but the maximum RMS torsional value of new bridge was 0.32°, this value is slightly higher than that of the 0.25° allowable limit of vibration recommended in the wind-resistant design manual for highway bridges in Japan (Sato 2003).

The new bridge showed the large amplitude in torsional motion as shown in Fig. 9(b). The large amplitude in torsional motion of new bridge effected to heave and torsional motion of existing bridge as show in Fig. 10(b). Therefore, the torsional frequency of 3.021 Hz of new bridge at mean speed of 23.63 m/s also appears in the existing bridge as show in Fig. 10b. The interference from new bridge affected to RMS vertical value of existing bridge was 1.09 cm. and RMS torsional value of existing bridge was 0.01°, these two values are significantly lower than those of the allowable limits of vibration recommended in the wind-resistant design manual for highway bridges in Japan (Sato 2003).

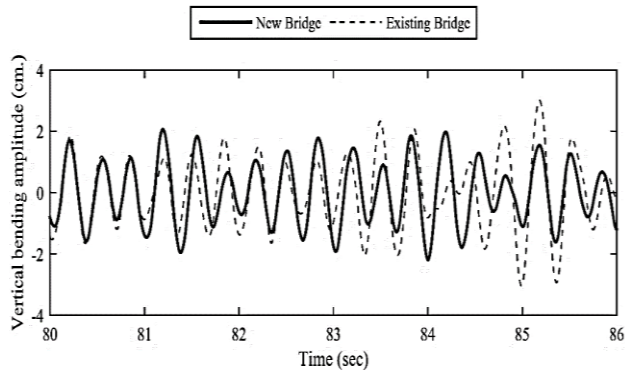

(a) Heave response

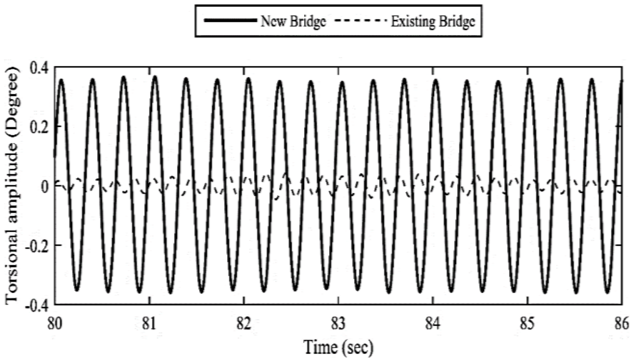

(b) Pitch response

Fig. 9 Vortex-induced vibration response of new and existing bridges for case 2 at mean wind speed of 23.63 m/s

6.2 Vortex induced vibration for the downstream new bridge and the upstream existing bridge (Case 3)

Fig. 11 show the RMS-velocity of new bridge and existing bridge in case 3, The VIV occurs at mean wind speed of 29.08 m/s, this vortex-shedding speed is relatively high. The vortex-shedding excitation was also shown in both vertical bending and torsional motion of existing bridge, which is located at upstream. The maximum RMS vertical value of existing bridge was 2.92 cm., this value is significantly lower than that of the 8.9 cm allowable limit of vibration recommended in the wind-resistant design manual for highway bridges in Japan (Sato 2003) but the maximum RMS torsional value of new bridge was 0.31°, this value is slightly higher than that of the 0.17° allowable limit of vibration recommended in the wind-resistant design manual for highway bridges in Japan (Sato 2003).

The existing bridge showed the large amplitude in torsional motion (see Fig. 12(b)). The large amplitude in torsional motion of existing bridge effected to heave and torsional motion of new bridge, as show in Fig. 13(a). Therefore, the torsional frequency of 4.936 Hz. of existing bridge at mean wind speed of 29.08 m/s also appears in the new bridge as shown in Fig. 13(a). The interference from existing bridge affected to RMS vertical value of new bridge was 0.74 cm. and RMS torsional value of existing bridge was 0.023°, these two values are significantly lower than those of the allowable limits of vibration recommended in the wind-resistant design manual for highway bridges in Japan (Sato 2003).

6.3 Comparison of the flutter response of new bridge from 3 configuration cases

Fig. 14 comparison the RMS-velocity (RMS-V) curve of new bridge from 3 cases. From the sectional bridge model test in wind tunnel under smooth winds, the response of new bridge from 3 configuration cased can be summarized as follows.

For the new bridge alone (case 1), the very abrupt transition with increasing velocity from the effectively zero torsional response amplitude to the clear instability occurs in the near neighborhood of mean wind speed of 81.84 m/s and completely flutter instability at mean wind speed of 87.09 m/s in prototype. The abrupt change in the vertical response at high wind speed is due to the effect of cross derivative H_2^* and H_3^*, which cause coupling of the torsional responses with the vertical response in term of damping and stiffness respectively (Boonyapinyo *et al*. 1999). It was found that the instability of the studied bridge model is the torsional flutter type. Since the studied bridge is the hard type flutter, the flutter instability has been defined as the mean wind speed at which this abrupt transition of torsional response was beginning in wind tunnel test or zero value of torsional damping ratio of the sectional model system. The stability limit is significantly high compared to the design wind speed.

For the new bridge located upstream and the existing bridge located downstream (case 2), the very abrupt transition with increasing velocity from the effectively zero torsional response amplitude to the clear instability occurs in the near neighborhood of mean wind speed of 70.18 m/s and completely flutter instability at mean wind speed of 75.35 m/s in prototype (see Figs. 15). It was found that the instability of the new bridge model is the torsional flutter type. The torsional spectral density of new bridge shows a huge alternating flutter as shows in Fig. 16(a). In this condition, the downstream existing bridge was subjected to galloping oscillations induced by the turbulent wake of upstream new bridge and it will be explained more detail in section 6.4. It should be noted that cases 2 result in significantly lower the flutter speed than cases 1.

When new bridge located downstream (case 3), the clear instability occurs in the near neighborhood of mean wind speed of 111.55 m/s and completely flutter instability at mean wind speed of 116.73 m/s in prototype. In cases 3, the new bridge shown the highest flutter speed from 3 configuration because the flutter speed of isolate existing bridge is significantly higher that of isolate new bridge (see Fig.17). The flutter instability of the new bridge reported that the similar torsional flutter type as case 1 and 2. The stability limit is extremely high compared to the design wind speed.

6.4 Comparison of the flutter response of existing bridge from 3 configuration cases

Fig. 17 comparison the RMS-velocity (RMS-V) curve of existing bridge from 3 cases. From the sectional bridge model test in wind tunnel under smooth winds, the response of existing bridge from 3 configuration cased can be

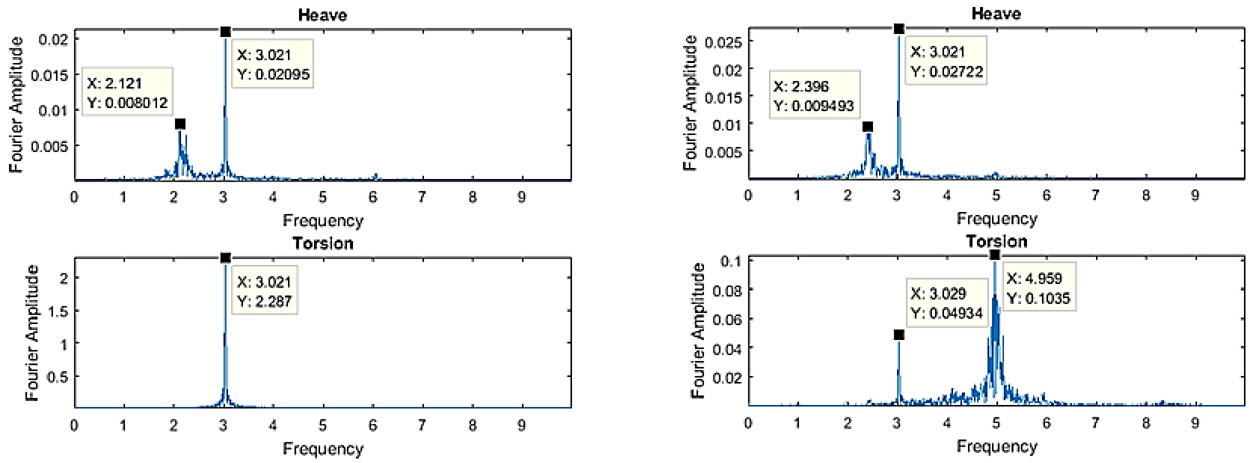

(a) New bridge (b) Existing bridge

Fig. 10 Fourier spectrum of new and existing bridges for case 2 at mean wind speed of 23.63 m/s

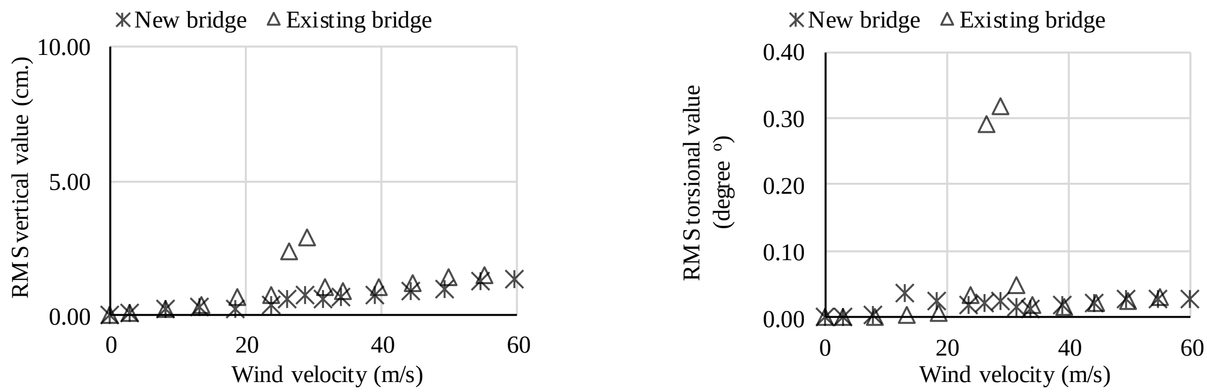

(a) Heave response (b) Pitch response

Fig. 11 RMS-velocity curve of new and existing bridges for case 3

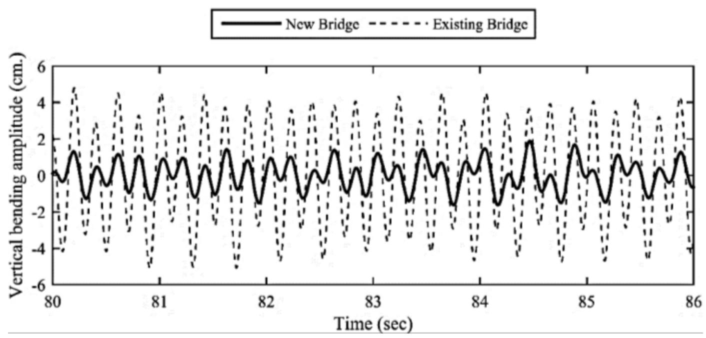

(a) Heave response

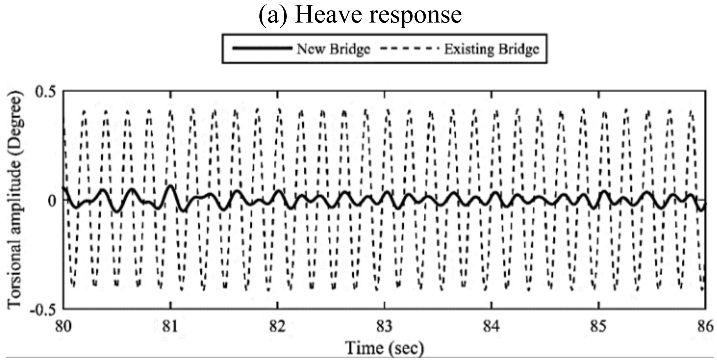

(b) Pitch response

Fig. 12 Vortex-induced vibration response of new and existing bridges for case 3 at mean wind speed of 29.08 m/s

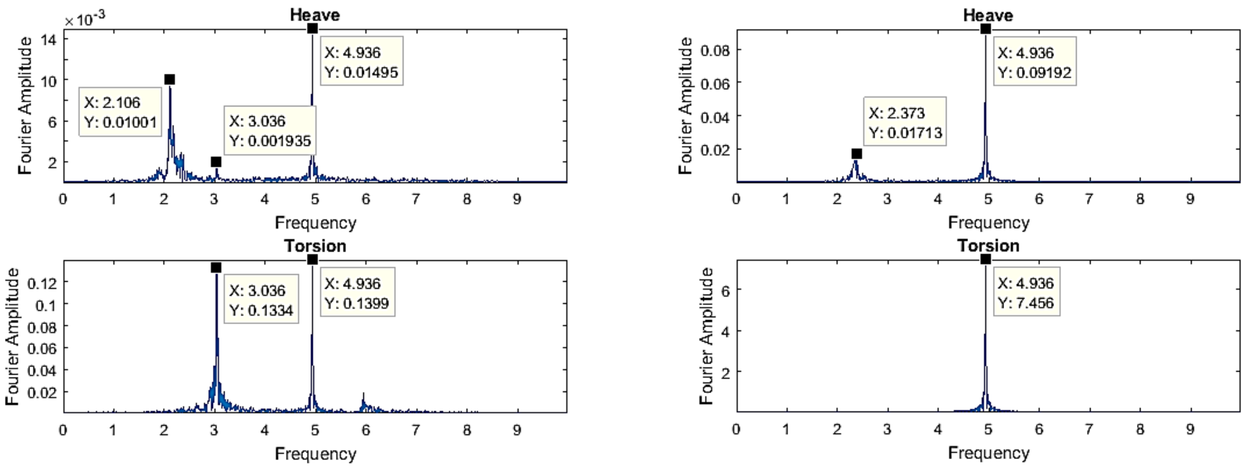

(a) New bridge (b) Existing bridge

Fig. 13 Fourier spectrum of new and existing bridges for case 3 at mean wind speed of 29.08 m/s

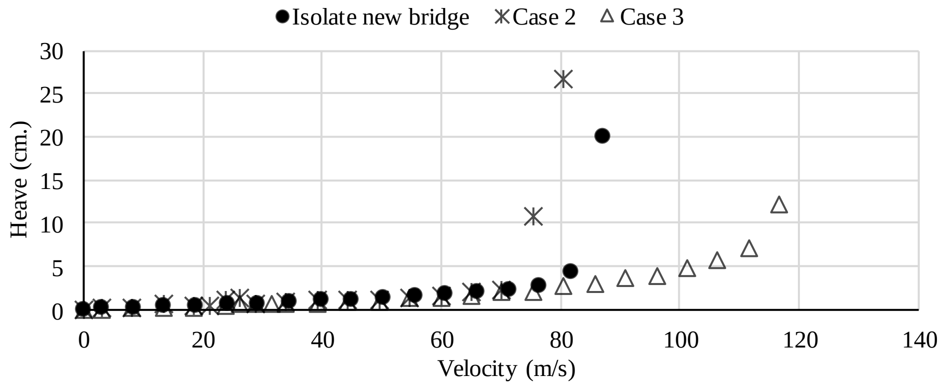

(a) Heave response

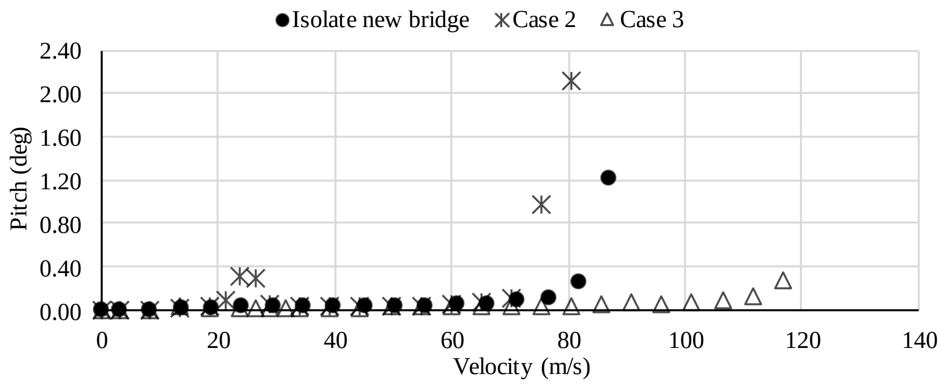

(b) Pitch response

Fig. 14 RMS-V curve of new bridge in 3 configuration cases

summarized as follows.

For the existing bridge alone, the very abrupt transition with increasing velocity from the effectively zero torsional response amplitude to the clear instability occurs in the near neighborhood of mean wind speed of 128.29 m/s and completely flutter instability at mean wind speed of 133.51 m/s in prototype. It was found that the instability of the studied bridge model is the torsional flutter type. The stability limit is significantly high compared to the design wind speed.

For the existing bridge located upstream and the new bridge located downstream (case 3), the very abrupt transition with increasing velocity from the effectively zero torsional response amplitude to the clear instability occurs in the near neighborhood of mean wind speed of 111.55 m/s and completely flutter instability at mean wind speed of 116.73 m/s in prototype (see Fig. 18). It was found that the flutter instability of the existing bridge is the torsional flutter type. The torsional spectral density of existing bridge shows a huge alternating flutter as shows in Fig. 19(b). The

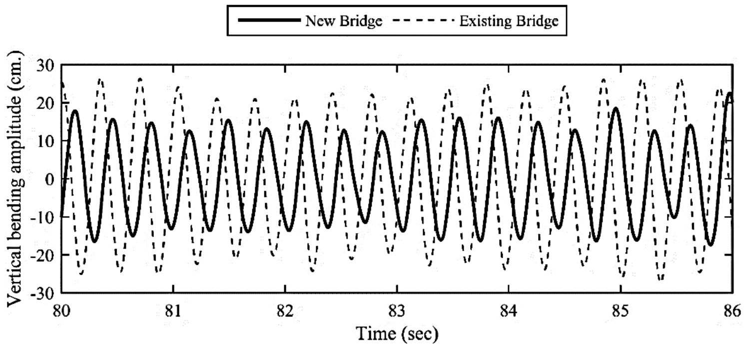

(a) Heave response

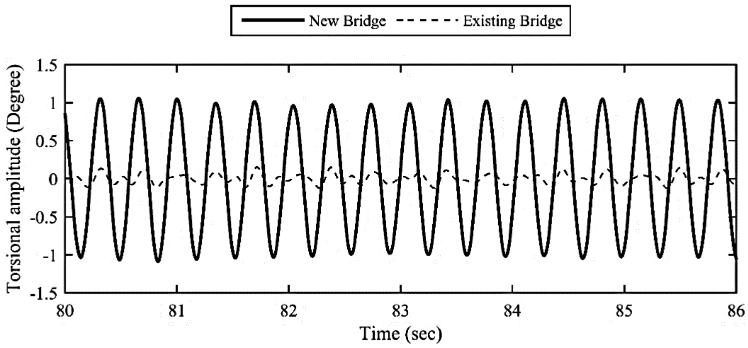

(b) Pitch response

Fig. 15 Flutter response of new and existing bridges for case 2 at mean wind speed of 75.35 m/s

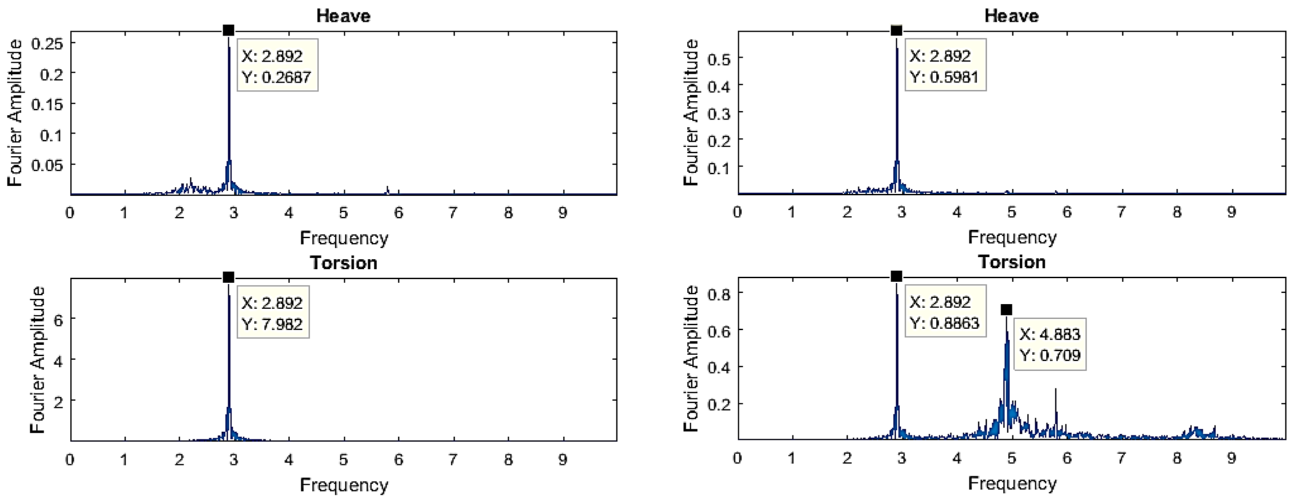

(a) New bridge (b) Existing bridge

Fig. 16 Fourier spectrum of new and existing bridges for case 2 at mean wind speed of 75.35 m/s

torsional frequency of upstream existing bridge 4.547 Hz induced downstream new bridge and resulted in torsional flutter of downstream new bridge. It should be noted that unlike case 3 of new bridge, case 3 of existing bridge result in significantly lower the flutter speed than the isolate existing bridge because of the interference effects of two bridges.

When existing bridge located downstream (case 2), the clear instability occurs in the near neighborhood of mean wind speed of 70.18 m/s and completely flutter instability at mean wind speed of 75.35 m/s in prototype. The torsional response of new bridge in Fig. 15(b) with torsional frequency of 2.892 Hz in Fig. 16(a) generated turbulent wakes flow and resulted in H_1^* of existing bridge in Fig.20 becomes zero at the reduced wind velocity (U/n_hB) of 6.82 corresponding to wind speed of 72.01 m/s (U =6.82*0.32*33 = 72.01 m/s). This flutter speed agrees well with RMS-V curve of existing bridge in Fig. 17. In this case, the existing bridge shown the lowest flutter speed from 3 configuration. It can clearly see in H_1^* of existing bridge in Fig. 20 that the downstream existing bridge was subjected to galloping oscillation induced by the turbulent wake of upstream new bridge. The galloping oscillation of the existing bridge only in case 2 but not via versus in case 3 are caused by the shape and size of the upstream new bridge. The new bridge has the open deck (see Figs. 2 and

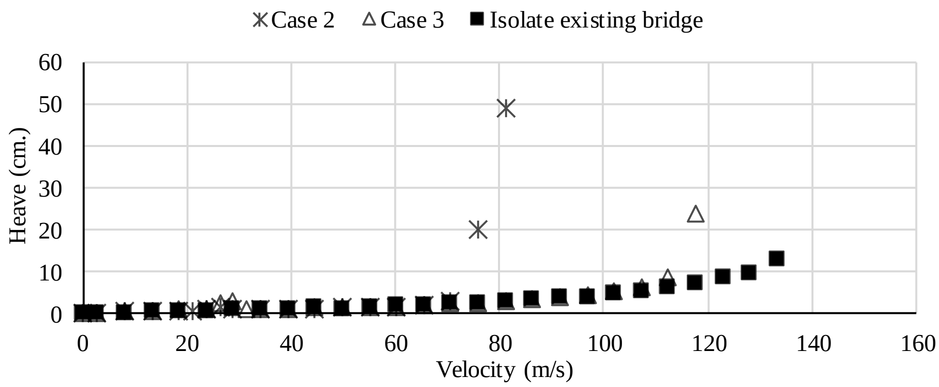

(a) Heave response

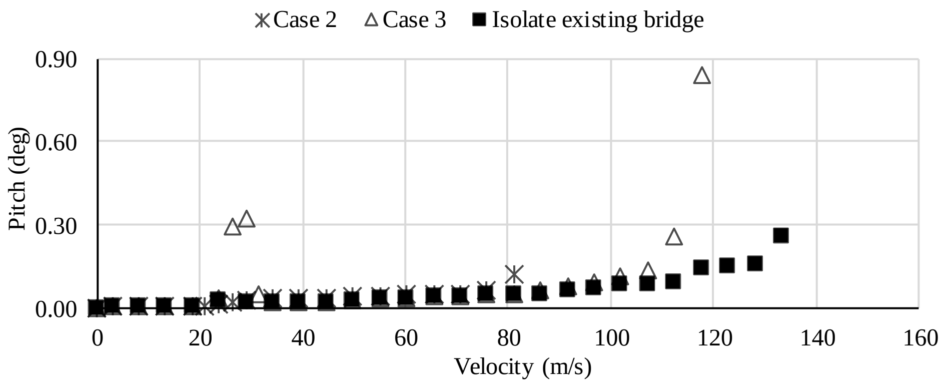

(b) Pitch response

Fig. 17 RMS-V curve of existing bridge in 3 configuration case

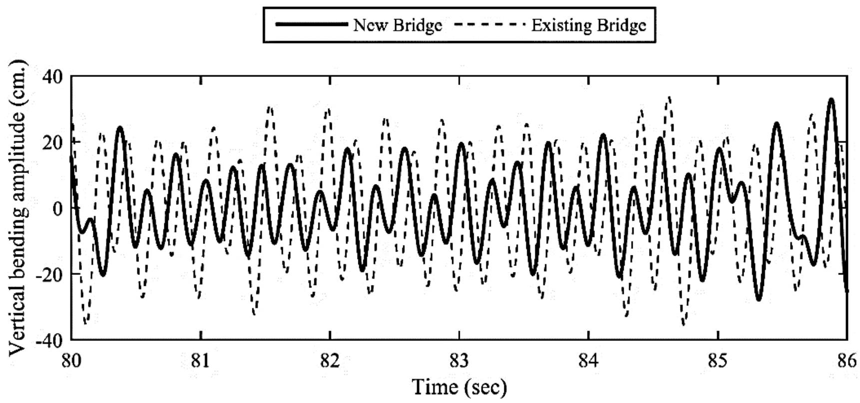

(a) Heave response

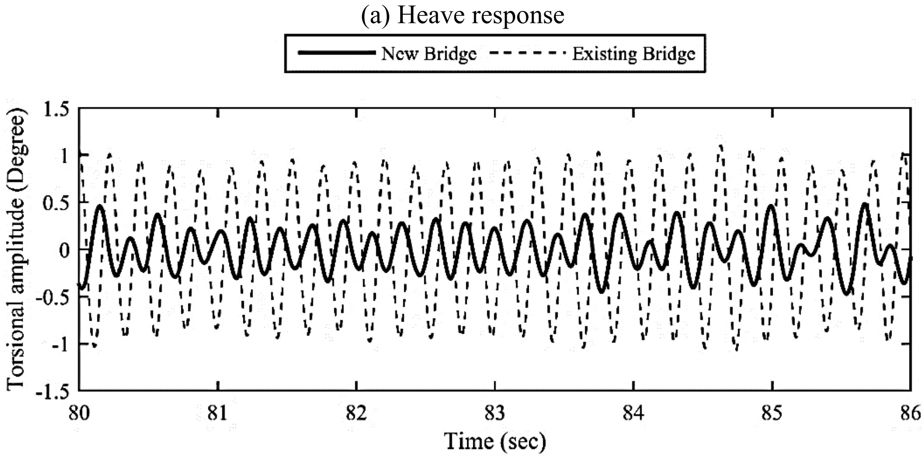

(b) Pitch response

Fig. 18 Flutter response of new and existing bridges for case 3 at mean wind speed of 116.73 m/s

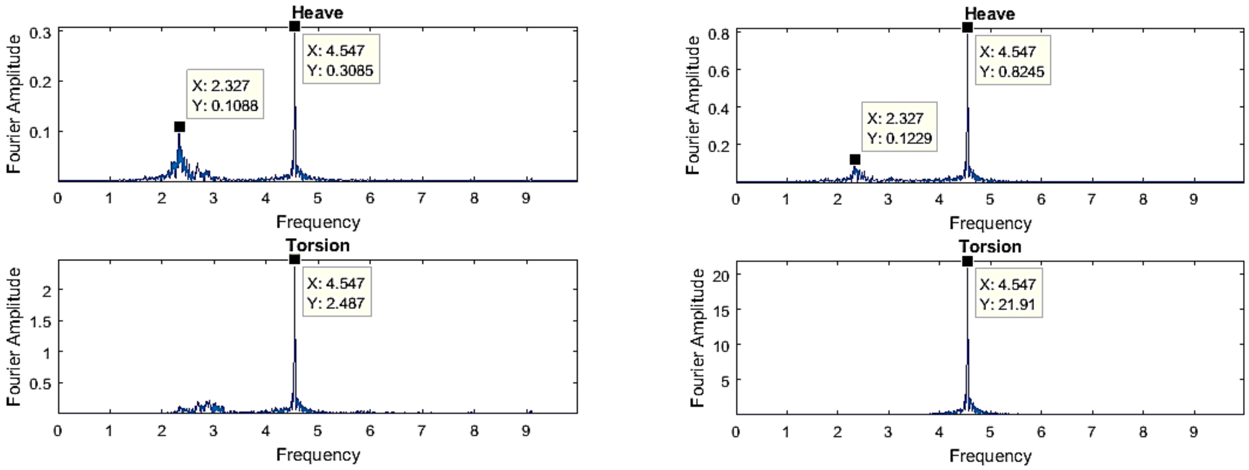

(a) New bridge (b) Existing bridge

Fig. 19 Fourier spectrum of new and existing bridges for case 3 at mean wind speed of 116.73 m/s

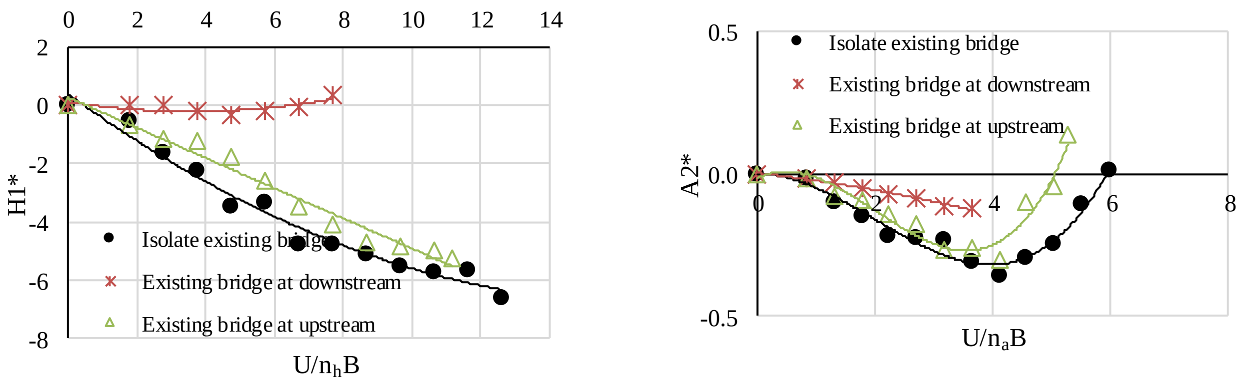

(a) (b)

Fig. 20 Comparisons of flutter derivatives H_1^* and A_2^* of the existing bridge in 3 configuration cases

4) and much wider deck than the existing deck (see Fig. 4).

7. Interference effects of two-parallel bridge decks on flutter derivative parameter

The eight-flutter derivatives (H_1^*- H_4^* and A_1^*- A_4^*) of new bridge from the sectional model test in wind tunnel for 3 cases under smooth wind are shown in Fig. 21. The non-dimensional parameters H_1^*, H_4^*, A_1^*, A_4^* are normalized with initial heave frequency of new bridge and H_2^*, H_3^*, A_2^*, A_3^* are normalized with initial torsional frequency of new bridge at any wind speeds as shown in Eq.1. The flutter derivatives were estimated from buffeting response by SSI-COV algorithm as presented in section 4. The interference effect of two-parallel bridge decks on flutter derivative parameter of new bridge can be summarized as follows.

The H_1^* derivative is related to the aerodynamic damping in the vertical motion. The increases of H_1^* derivative in negative value for 3 configurations cases reported that the new bridge is not sensitive to vertical instability. Therefore, the studied bridge is stable with respect to the 1DOF vertical motion. The H_1^* derivative in case 3 has the most vertical aerodynamic damping among 3 configuration cases. The H_2^*, H_4^* derivative are sensitive to noise as show in Fig. 21 (Gu *et al*. 2001, Pospíšil *et al*. 2016). The value of H_4^* derivative is negative and the magnitudes increase with the reduced velocities.

The A_2^* derivative is related to the aerodynamic damping of torsion, which is very critical to flutter instability. The change from negative value to close to zero in higher reduced wind speeds suggest that there is possibility that the bridge becomes to the torsional flutter instability. The new bridge located at upstream (case 2) is the most vulnerable to torsional flutter instability, because the A_2^* becomes positive at the lowest reduced wind velocity (U/n_aB=4.00, U =4.00*0.416*42.4 =70.51 m/s) in comparison with case 1 (U/n_aB=4.59, U =4.59*0.416*42.4 =80.90 m/s) and case 3 (U/n_aB=6.35, U =6.35*0.416*42.4 =112.08 m/s). The torsional speeds calculated from A_2^* agree well with aeroelastic response from section 6.3 for 3 configuration cases.

The A_3^* derivative is positive and the magnitudes increase with the reduced velocities. The trend of A_3^* derivative was similar to A_2^*. The A_3^* derivative demonstrate that the configuration of new bridge significantly modifies generalized oscillation frequency in high reduced wind speed of the wind-parallel-bridge system.

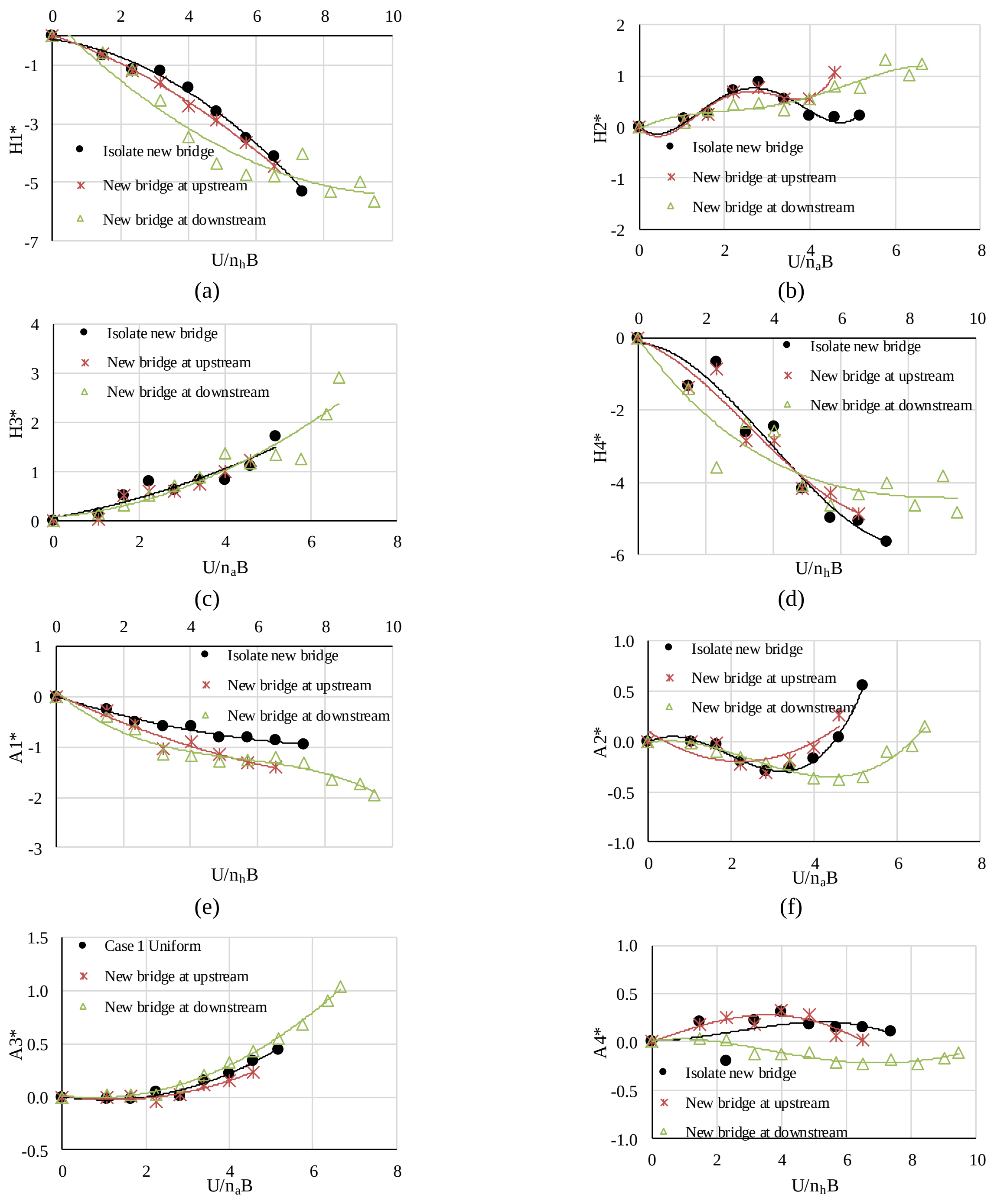

Fig. 21 Comparisons of flutter derivatives of the new bridge in 3 configuration cases

The values of A_4^* for 3 configuration cases are small. The torsional aerodynamic stiffness coefficients A_4^* in case 3 are in negative values. This means stiffening torsional stiffness of the downstream new bridge.

8. Conclusions

The interference effects on aerodynamic coefficients, vortex induced vibration, flutter instability and flutter derivative of parallel cable-stayed bridges were investigated by wind tunnel tests. The two-parallel cable-stayed bridges are closed to each other, which have significant difference in cross sections, dynamic properties, and flutter speeds of each isolate bridges. The large-scale model (1:90) can create geometric accuracy which suitable for measuring aerodynamic static and aeroelastic responses of the two parallel bridge decks. The two section models were installed in the dynamic supported to allow heaving and torsional 2DOF motion for both models. An advanced covariance-driven stochastic subspace identification technique (SSI-COV) was used to estimate flutter derivatives from buffeting responses under smooth wind. From wind tunnel tests, the conclusion can be summarized as follows.

The interference effects on aerodynamic coefficients of new bridge.

• Interference effects of two bridges decks on aerodynamic coefficients of new bridge depend on a girder shape, a gap distance between parallel deck, and an angle of wind attack. As a result, drag coefficient of the new bridge in parallel configurations was less than that in the isolate new bridge. The drag coefficient of case 3 has dropped significantly because the new bridge was sheltered by an existing bridge. The lift coefficient of new bridge in parallel configurations and the isolate new bridge showed the same trend. The torsion coefficient of the new bridge in parallel configurations was similar to the isolate new bridge.

The interference effects on VIV.

• The isolate new bridge and the isolate existing bridge showed no problem in VIV.

• The main interference effect on VIV of the new bridge occurs when the new bridge located at upstream (case 2), which relatively high vortex-shedding speed. The new bridge showed a VIV for a torsional motion. The RMS torsional value of new bridge exceeds the recommend value given by the wind-resistant design manual for highway bridges in Japan (Sato, 2003). The aeroelastic interference between two parallel bridge deck was significantly resulted in VIV of the upstream decks.

• When the existing bridge located at upstream (case 3), it showed a conventional VIV for heaving and torsional motions at relatively high mean wind speed. The RMS torsional value of existing bridge exceeds the recommend value given by the wind-resistant design manual for highway bridges in Japan (Sato 2003).

The interference effects on flutter instability.

• The 75.35 m/s flutter speed of the new bridge located at upstream (case 2) was lower than 87.09 m/s of the new bridge alone (case 1). The flutter instability of the new bridge in case 1 and 2 are the torsional flutter type.

• The huge torsional motion from upstream new bridge (case 2) generated turbulent wakes flow and resulted in $H_1^*$of existing bridge (Fig. 20) becomes zero at the reduced wind velocity (U/n_hB) of 6.82 corresponding to wind speed of 72.01 m/s (U=6.82*0.32*33=72.01 m/s). In this case, the downstream existing bridge was subjected to galloping oscillation induced by the turbulent wake of upstream new bridge. The galloping oscillation of the existing bridge only in case 2 but not via versus in case 3 are caused by the shape and size of the upstream new bridge. The new bridge has the open deck and much wider deck than the existing deck.

• The 116.73 m/s flutter speed of the existing bridge located at upstream (case 3) was significantly lower than 128.29 m/s of the existing bridge alone. The flutter instability of the existing bridge is the torsional flutter type. The new bridge also results in significant reduction of the flutter speed of existing bridge from the 128.29 m/s flutter speed of the isolated existing bridge to the 75.35 m/s flutter speed of downstream existing bridge.

The interference effects on flutter derivative of new bridge.

• The parallel configuration of new bridge significantly modifies A_2^* derivative in high reduced wind speed. The reduced wind speed for A_2^* significantly decreased from 4.59 for isolate new bridge to 4.00 for upstream new bridge. As a result, the new bridge located at upstream (case 2) is the most vulnerable to torsional flutter instability.

Since the bridges are located in parallel configuration, their wind induced response becomes more complex than the single stand-alone bridge. Therefore, results from the wind tunnel test are necessary to identify and measure aeroelastic problems.

Acknowledgments

The authors wish to express their sincere appreciations to Epsilon Co. Ltd. in Association with Wiecon Co. Ltd., and Expressway Authority of Thailand for their financial supports in wind tunnel test. The scholarship for Ph.D. Student of Faculty of Engineering, Thammasat University to the first author is also acknowledged.

References

AES Group, Kinematics and OPAC (2001), “The Rama IX Bridge Tenth-Year Inspection”, Submitted to Expressway and Rapid Transit Authority of Thailand

Andersen, S.A., Øiseth, O., Johansson, J. and Brandt, A. (2018), “Flutter derivatives from free decay tests of a rectangular B/D=10 section estimated by optimized system identification methods”, *Eng. Struct.,* **156**, 284-293, https://doi.org/10.1016/j.engstruct.2017.11.059

Argentini, T., Rocchi, D. and Zasso, A. (2015), “Aerodynamic interference and vortex-induced vibrations on parallel bridges: The Ewijk bridge during different stages of refurbishment”, *J. Wind Eng. Ind. Aerod.*, **147**, 276-282. http://dx.doi.org/10.1016/j.jweia.2015.07.012

Boonyapinyo, V., Yamada, H. and Miyata, T. (1994), “Wind-induced nonlinear lateral- torsional buckling of cable-stayed bridges”, *J.Struct. Eng.*, **120**(2), 486-506. https://doi.org/10.1061/(ASCE)0733-9445(1994)120:2(486).

Boonyapinyo, V., Miyata, T. and Yamada, H. (1999), “Advanced aerodynamic analysis of suspension bridges by state-space approach”, *J.Struct. Eng.*, **125**(12), 1357-1366. https://doi.org/10.1061/(ASCE)0733-9445(1999)125:12(1357).

Boonyapinyo, V., Lauhatanon, Y. and Lukkunaprasit, P. (2006), “Nonlinear aerostatic stability analysis of suspension bridges”, *Eng. Struct.*, **28**(5), 793-803. https://doi.org/10.1016/j.engstruct.2005.10.008.

Boonyapinyo V., Janesupasaeree T. and Thamasungkeeti W. (2009), “Identification of flutter derivatives of bridge decks by stochastic subspace method”, *The 7th Asia-Pacific Conference on Wind Engineering*, Taipei, November.

Boonyapinyo, V. and Janesupasaeree, T. (2010), “Data-driven stochastic subspace identification of flutter derivatives of bridge decks”, *J. Wind Eng. Ind. Aerod.*, **98**(12), 784-799. https://doi.org/10.1016/j.jweia.2010.07.003.

Dallaire, P.O., Taylorb, Z.J. and Stoyanoffc, S. (2016), “Sectional

model tests of tandem bridge decks in dynamic suspension systems", *In the 8th International Colloquium on Bluff Body Aerodynamics and Applications*., Massachusetts, U.S.A, June.
Dragomirescu, E., Wang, Z. and Hoftyzer, M. (2016), "Aerodynamic characteristics investigation of Megane multi-box bridge deck by CFD-LES simulations and experimental tests", *Wind Struct*., **22**(2), 161-184. https://doi.org/10.12989/was.2016.22.2.161.
Ehsan, F. and Scanlan, R.H. (1990), "Vortex-induced vibrations of flexible bridges", *J. Eng. Mech*., **116**(6), 1392-1400. https://doi.org/10.1061/(ASCE)0733-9399(1990)116:6(1392).
Epsilon Co. Ltd. and Weicon Co. Ltd. (2016), "EXAT Bridge Project: Mode Shape of Structure", Thailand.
Gu, M., Zhang, R. and Xiang, H. (2001), "Parametric study on flutter derivatives of bridge decks", *Eng. Struct*., **23**(12), 1607-1613. https://doi.org/10.1016/S0141-0296(01)00059-1
Gu, M. and Qin, X.R. (2004), "Direct identification of flutter derivatives and aerodynamic admittances of bridge decks", *Eng. Struct*., **26**(14), 2161-2172. https://doi.org/10.1016/j.engstruct.2004.07.015.
Hu, C., Zhou, Z. and Jiang, B. (2019), "Effects of types of bridge decks on competitive relationships between aerostatic and flutter stability for a super long cable-stayed bridge", *Wind Struct*., **28**(4), 255-270. https://doi.org/10.12989/was.2019.28.4.255
Irwin, P., Stoyanoff, S., Xie, J. and Hunter, M. (2005), "Tacoma narrows 50 years later-wind engineering investigations for parallel bridges", *Bridge Struct*., **1**(1), 3-17. https://doi.org/10.1080/1573248042000274551
Kimura, K., Shima, K., Sano, K., Kubo, Y., Kato, K. and Ukon, H. (2008), "Effects of separation distance on wind-induced response of parallel box girders", *J. Wind Eng. Ind. Aerod*., **96**(6-7), 954-962. http://dx.doi.org/10.1016/j.jweia.2007.06.021.
Kim, S.J., Kim, H.K., Calmer, R., Park, J., Kim, G.S. and Lee, D.K. (2013), "Operational field monitoring of interactive vortex-induced vibrations between two parallel cable-stayed bridges", *J. Wind Eng. Ind. Aerod*., **123**, 143-154. http://dx.doi.org/10.1016/j.jweia.2013.10.001.
Laima, S., Wu, B., Jiang, C., Chen, W. and Li, H. (2019), "Numerical study on Reynolds number effects on the aerodynamic characteristics of a twin-box girder", *Wind Struct.*, **28**(5), 285-298. https://doi.org/10.12989/was.2019.28.5.285
Larsen, S.V., Astiz, M.A. and Larose, G.L. (2000), "Aerodynamic interference between two closely spaced cable supported bridges", *In the 4th International Colloquium on Bluff Body Aerodynamics and Applications*, Bochum, Germany, September.
Liu, Z., Chen, Z., Liu, G. and Shao, X. (2009), "Experimental study of aerodynamic interference effects on aerostatic coefficient of twin deck bridges", *Front. Archit. Civ. Eng. China*, **3**(3), 292-298. https://doi.org/10.1007/s11709-009-0048-8
Meng, X., Zhu, L. and Guo, Z. (2011), "Aerodynamic interference effects and mitigation measures on vortex-induced vibrations of two adjacent cable-stayed bridges", *Front. Archit. Civ. Eng. China*, **5**(4), 510-517. https://doi.org/10.1007/s11709-011-0129-3
Park, J., Kim, S. and Kim, H.K. (2017), "Effect of gap distance on vortex-induced vibration in two parallel cable-stayed bridges", *J. Wind Eng. Ind. Aerod.*, **162**, 35-44. http://dx.doi.org/10.1016/j.jweia.2017.01.004
Park, J. and Kim, H.K. (2017), "Effect of the relative differences in the natural frequencies of parallel cable-stayed bridges during interactive vortex-induced vibration", *J. Wind Eng. Ind. Aerod.*, **171**, 330-341. https://doi.org/10.1016/j.jweia.2017.10.010.
Pospíšil, S., Buljac, A., Kozmar, H., Kuznetsov, S., Machácek, M. and Král, R. (2016), "Influence of stationary vehicles on bridge aerodynamic and aeroelastic coefficients", *J. Bridge Eng.*, **22**(4), 05016012.
Sato, H. (2003), "Wind-resistant design manual for highway bridges in Japan", *J. Wind Eng. Ind. Aerod*., **91**(12-15), 1499-1509. https://doi.org/10.1016/j.jweia.2003.09.012.
Seo, J.W., Kim, H.K., Park, J., Kim, K.T. and Kim, G.N. (2013), "Interference effect on vortex-induced vibration in a parallel twin cable-stayed bridge", *J. Wind Eng. Ind. Aerod*., **116**, 7-20. http://dx.doi.org/10.1016/j.jweia.2013.10.001.
Simiu, E. and Scanlan, R.H. (1996), "Wind Effects on Structures", John Wiley, New York, U.S.A.
Wang, K., Liao, H. and Li, M. (2016), "Flutter suppression of long-span suspension bridge with truss girder", *Wind Struct*., **23**(5), 405-420. https://doi.org/10.12989/was.2016.23.5.405
Zhang, Z.T. and Chen Z.Q. (2011), "Similarity of amplitude of sectional model to that of full bridge in the case of vortex-induced resonance", *China Civil Eng. J.*, **44**(7), 77-82.
Zhu, L.D. (2005), "Mass simulation and amplitude conversion of bridge sectional model test for vortex-excited resonance", *Eng. Mech.*, **22**(5), 204-208.

AD